Dual-Function Cobalt-Nickel Nanoparticles Tailored for High-Temperature Induction-Heated Steam Methane Reforming

Vinum, Morten G.; Almind, Mads Radmer; Engbaek, Jakob S.; Vendelbo, Søren Bastholm; Hansen, Mikkel F.; Frandsen, Cathrine; Bendix, Jesper; Mortensen, Peter M.

Published in:
Angewandte Chemie

Link to article, DOI:
10.1002/ange.201804832

Publication date:
2018

Document Version
Publisher's PDF, also known as Version of record

Heterogeneous Catalysis

International Edition: DOI: 10.1002/anie.201804832
German Edition: DOI: 10.1002/ange.201804832

Dual-Function Cobalt–Nickel Nanoparticles Tailored for High-Temperature Induction-Heated Steam Methane Reforming

Morten G. Vinum, Mads R. Almind, Jakob S. Engbæk, Søren B. Vendelbo, Mikkel F. Hansen, Cathrine Frandsen, Jesper Bendix,* and Peter M. Mortensen**

Abstract: *The tailored chemical synthesis of binary and ternary alloy nanoparticles with a uniform elemental composition is presented. Their dual use as magnetic susceptors for induction heating and catalytic agent for steam reforming of methane to produce hydrogen at temperatures near and above 800 °C is demonstrated. The heating and catalytic performance of two chemically synthesized samples of* ***CoNi*** *and* ***Cu⊂CoNi*** *are compared and held against a traditional Ni-based reforming catalyst. The structural, magnetic, and catalytic properties of the samples were characterized by X-ray diffraction, elemental analysis, magnetometry, and reactivity measurements. For induction-heated catalysts, the conversion rate of methane is limited by chemical reactivity, as opposed to the case of traditional externally heated reformers where heat transport limitations are the limiting factor. Catalyst production by the synthetic route allows controlled doping with miniscule concentrations of auxiliary metals.*

Direct heating of magnetic nanoparticles (NPs) by magnetic induction, including using magnetic hysteresis heating, holds many potential advantages over conventional heating as it allows for a vast number of new approaches to otherwise difficult tasks. The most prominent of these are drug release,[1,2] control of single-cell functions,[3] and disease treatment by hyperthermia.[4,5] While a collective feature of all these applications is the aim towards medical use, only few examples exist of industrial applications of magnetically heated NPs.[6] Herein, we present the preparation and implementation of a novel nanostructured material for hydrogen production via endothermic steam reforming of methane (SMR) using solely induction heating as energy source.[7]

Hydrogen is by far the most produced chemical worldwide on a molar basis.[8] To accommodate an ever-growing demand, efforts have been made to generate hydrogen from biofuels, electrolysis, wind, solar, and nuclear energy. The most affordable and efficient way to generate hydrogen is still various forms of steam reforming of hydrocarbons from fossil fuels.[9] The SMR takes place according to Equations (1) and (2):

$$CH_4 + H_2O \rightleftharpoons 3\,H_2 + CO \qquad (\Delta H^\circ = 206.15\,\mathrm{kJ\,mol^{-1}}) \tag{1}$$

$$CO + H_2O \rightleftharpoons H_2 + CO_2 \qquad (\Delta H^\circ = -41.16\,\mathrm{kJ\,mol^{-1}}) \tag{2}$$

This overall endothermic reaction presents a challenge as it is only thermodynamically favored at temperatures approaching 700 °C at ambient conditions, and even higher temperatures of 950 °C are needed in industry owing to the high operational pressures used.[10]

A typical SMR plant for production of hydrogen generally consists of a pre-reformer followed by a tubular reformer, a shift converter, and final product purification (typically done by pressure swing adsorption (PSA)) in combination with expensive heat-exchange coils to minimize heat loss.[11] A long-standing challenge in hydrogen production has been the excessive heating needed in the reforming section of the current design, which, due to costly waste-heat sections, favors large-scale plants to achieve a feasible reforming economy. Usually, energy delivered to the reactor bed from the fired section is only around 50 %, the rest is recovered in the flue gas.[10,12] This however dictates, that a significant amount of energy is spent outside of the actual reaction chamber. Additionally, the start-up time of such plants is often on the order of a few days to ensure controlled heating of the large tubes with minimum risk of tube rupture. In stark contrast, induction heating provides rapid and efficient heating of ferromagnetic materials, and potentially the heat can be delivered directly in the catalyst, if such a magnetic catalyst can be realized. This requires special radiofrequency transparent reactors to avoid shielding effects between the catalyst and the induction coil. In a future hydrogen economy, we therefore envision induction-heated reforming as a small-scale hydrogen production technology with a fast start-up for ad hoc on-site supply of hydrogen.

Previously, induction heating of ferromagnetic Fe-based NPs was utilized in a liquid phase organic synthesis flow

[*] M. G. Vinum, Dr. P. M. Mortensen
Haldor Topsøe A/S
Nymøllevej 55, 2800 Kgs. Lyngby (Denmark)
E-mail: morten.vinum@chem.ku.dk
pmor@topsoe.com
M. G. Vinum, Prof. Dr. J. Bendix
Department of Chemistry, University of Copenhagen
2100 Copenhagen (Denmark)
E-mail: bendix@kiku.dk
M. R. Almind, Prof. Dr. C. Frandsen
DTU Physics, Technical University of Denmark
2800 Kgs. Lyngby (Denmark)
Dr. J. S. Engbæk, Dr. S. B. Vendelbo
Danish Technological Institute
2630 Taastrup (Denmark)
Dr. M. F. Hansen
DTU Nanotech, Technical University of Denmark
2800 Kgs. Lyngby (Denmark)
Supporting information and the ORCID identification number(s) for the author(s) of this article can be found under: https://doi.org/10.1002/anie.201804832.

reactor in a series of pioneering studies,[13–15] although the NPs were only used for heating and did not supply a catalytic function. Others have later made research into magnetic zeolites and related systems, where NiFe-based particles may also play a catalytic role.[16,17] More recently, others reported iron-based core–shell NPs doped with precious metals as candidates for induction heated heterogeneous catalysis.[18,19] However, in case of SMR with reaction temperatures around 800 °C, iron with a Curie temperature, T_C, of 770 °C is not suitable as magnetic susceptor. The only element with a higher T_C than iron is cobalt ($T_C = 1115$ °C)[20] and hence for induction heated SMR, the magnetic susceptor must be based on Co and alloys thereof.

Oxidation of Co readily takes place at the high temperatures and partial pressures of water relevant to the SMR process, and a significant challenge is to avoid oxidation of Co as this leads to the formation of antiferro- and paramagnetic phases.[21,22] Alloying with Ni provides a dual solution to this as Ni is an excellent catalyst for endothermic SMR, and Ni stabilizes the Co phase against oxidation while maintaining activities similar to that of pure Ni.[22] Recently, we had some success with this idea in a proof-of-concept showing that it was indeed possible to heat such alloyed NPs to temperatures approaching the desired range, and to produce hydrogen at these elevated temperatures. However, owing to the serendipity of sequential impregnation used in the previous study, control over the microscopic metal distribution had to be renounced, evidenced by the large differences found in alloy compositions in that study, leaving only a small fraction with high T_C and a very small hysteresis opening (see below) accessible for the purpose of heating.[23–25]

Herein, to take control at the molecular level, we conceptually changed the approach to catalyst manufacture, by preparing both active NPs and inert carrier by a chemical synthesis route, with the aim of producing more stable and uniform NPs, accessible in the desired temperature regime. Forming the catalyst precursor in solution and then precipitating it by addition of base, guaranteed the homogeneity of the material. Subsequently, the material was reduced, hereby directly producing catalytic nanoparticles within a porous non-active carrier material. To benchmark the activity of the formed catalyst, we also synthesized a traditional Ni catalyst on $MgAl_2O_4$ support by the same route with a loading of 15 wt% Ni (**1**) as a reference, to mimic commercially available reforming catalyst,[10] denoted **Ni-ref** (Supporting Information, Table S1, Figure S1).

The synthetic procedure (see the Supporting Information and Figure S2 therein) uniformly gave a homogeneous compound, which could be tuned to accommodate a vast range of metals at different ratios. The initial precipitate was shown by XRD to consist of a spinel-type phase of $M_yCo_{(1-x-1/2y)}Ni_{(x-1/2y)}Al_2O_4$ (where M = Cr, Mn, Fe, Cu as shown in the Supporting Information, Table S1, Figure S3). Here, we chose to focus on just two chemically synthesized samples, one un-doped sample with $x = 0.5$ (**2a**) hereafter **CoNi**, and a Cu-doped sample with $x = 0.5$ and $y = 0.01$ (**2b**) hereafter **Cu⊂CoNi** (Table 1). Following reduction of both samples in hydrogen, peaks originating from *fcc*-Co/Ni (Supporting Information, Figures S4 and S5) were identifiable in the XRD patterns of both **CoNi** and **Cu⊂CoNi** indicating the formation of metallic NPs, as well as γ-Al_2O_3 (both cubic and tetragonal phases) by the degradation of the original spinel structure. No evidence of non-reduced starting material was found in the final samples.

Table 1: Selected properties of samples **1**, **2a**, and **2b**.

Sample (Name)	Composition	Activity[a] [mol g^{-1} h^{-1}]	T_C [°C]	Ni-TOF[a] [s^{-1}]
1 (Ni-ref)	$^{15.0\,wt\%}Ni⊂MgAl_2O_4$	0.440	355[b]	0.584
2a (CoNi)	$Co_{0.5}Ni_{0.5}⊂Al_2O_3$	0.184	892[b]	0.435
2b (Cu⊂CoNi)	$^{0.36\,wt\%}Cu⊂2a$	0.244	875[b]	0.535

[a] Measured at 450 °C. [b] Estimated via the two-tangent method applied to the magnetic moment vs. temperature plots (see the Supporting Information and Figure S10 therein).

120 kV scanning transmission electron microscopy (STEM) high-angle annular dark field (HAADF) images were used in combination with electron dispersive X-ray spectroscopy (EDS) to map and evaluate the nature and composition of the NPs of **CoNi** and **Cu⊂CoNi** formed on the surface of the alumina support by the reduction process (Figure 1). From this, an average length/width of ca. 44/ca. 36 nm and ca. 54/ca. 43 nm, were evaluated for **CoNi** and **Cu⊂CoNi**, respectively (Supporting Information, Figure S6).

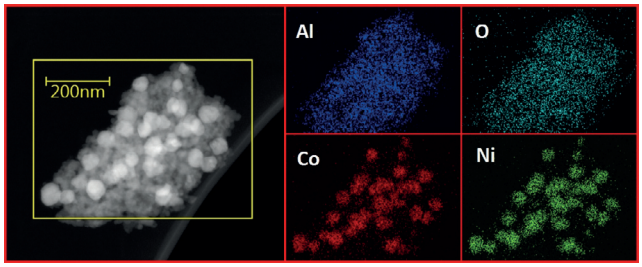

Figure 1. Left: STEM-HAADF image of a freshly prepared sample of **CoNi**. Right: Elemental mapping of Al (purple), O (teal), Co (red), and Ni (green) using EDS analysis of the same sample. Co wt% determined by EDS analysis for **CoNi** is presented in Figure 2.

These results are consistent with the crystallite sizes of 20–30 nm estimated from XRD analysis using the Scherrer equation, considering the uncertainties associated with this (Supporting Information, Table S1, see the Supporting Information for further comments).

The EDS analysis revealed an even distribution of Ni and Co throughout the nanoparticles (more than 40 NPs were individually addressed per sample) with an average Co content of each NP of 52.9 wt% (±5.8 wt%) in sample **CoNi** (Figure 2) and 52.9 wt.% (±3.0 wt%) in sample **Cu⊂CoNi** (Supporting Information, Figures S7–S9), close to the stoichiometric ratio defined by the synthetic route.

Measurements using a traditional externally heated setup dedicated for steam reforming activity measurements revealed a steam reforming activity for **CoNi** of 40% of that for **Ni-ref**. Chemically tuning the activity with miniscule dopings of Cu (**Cu⊂CoNi**) increased the performance significantly to reach 55%. In terms of turn over frequency (TOF)

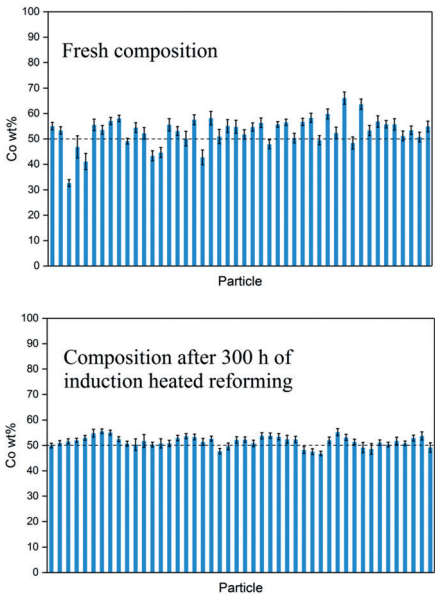

Figure 2. Top: Weight percentage of Co throughout individual NPs in **CoNi**. Bottom: Composition of the same sample after a 300 h induction heated steam reforming experiment (see Figure 6). The dashed line at 50 wt% represents the nominal composition.

per exposed metal site (taking the size and metal distribution into account), the TOFs of **CoNi** and **Cu⊂CoNi** were found to 75% and 91% of that of **Ni-ref,** respectively (Table 1). The observation that miniscule doping with Cu promotes activity of Ni catalysts in SMR concurs with previous results[26] and additional results obtained by traditional activity measurements (Supporting Information, Table S1). Any possible support related effects on the activity was not studied herein.

The magnetic moment of **CoNi** and **Cu⊂CoNi** was measured versus temperature in a small applied magnetic field of 10 mT to determine the effective Curie temperature of the samples as well as to check for the presence of multiple magnetic phases (Figure 3). At temperatures below 800 °C, the nanomaterial acted as a ferromagnet with a slow decrease of the magnetic moment upon heating. Above this temperature, the moment decreased more rapidly and reached a value close to zero at the maximum measurement temperature of 950 °C. Effective Curie temperatures for **CoNi** and **Cu⊂CoNi** were determined to $T_C = 892$ °C and 875 °C, respectively (see the Supporting Information). The single rapid decrease in moment around 850 °C or 825 °C indicates a homogenous material with a narrow alloy composition in both samples in agreement with EDS results. The smaller T_C for **Cu⊂CoNi** relative to **CoNi** despite similar composition in EDS may be due to the small content of nonmagnetic Cu which was not evaluated by EDS.

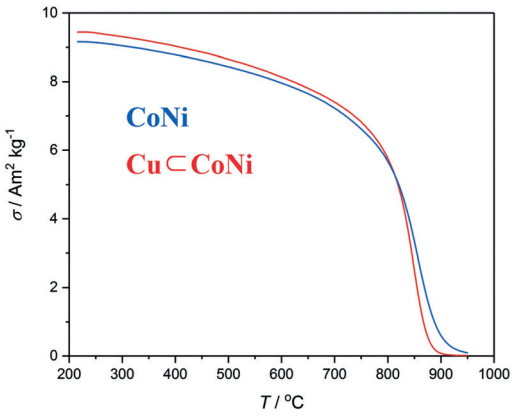

Figure 3. Magnetic moment versus temperature of **CoNi** and **Cu⊂CoNi**. The sample was measured in an applied magnetic field of $B_{app} = 10$ mT at temperatures decreasing from 950 °C to 200 °C at 5 °C min^{-1}. Apparent solid lines are actual data points.

Moreover, hysteresis measurements of **CoNi** and **Cu⊂CoNi** in maximum applied magnetic fields B_{max} ranging from 5 mT to 55 mT were conducted isothermally between temperatures of 200 °C and 950 °C in increments of 50 °C (Supporting Information, Figures S11–S14). The area of the hysteresis loop is defined as:

$$W_H = \oint_{B_{max}} \sigma(B_{app}) \mathrm{d}B_{app} \quad (3)$$

where σ [A m^2 kg^{-1}] is the specific magnetization (magnetic moment per sample mass), indicates the heat generated per cycle in units of J kg^{-1} upon cycling the applied magnetic field between $+B_{max}$ to $-B_{max}$ and back (Figure 4). From the measurements conducted on **CoNi,** it is clear that W_H is still appreciably different from zero at temperatures above 800 °C at moderate values of B_{max}. This suggests the possibility of using magnetic hysteresis heating at and above this temperature.

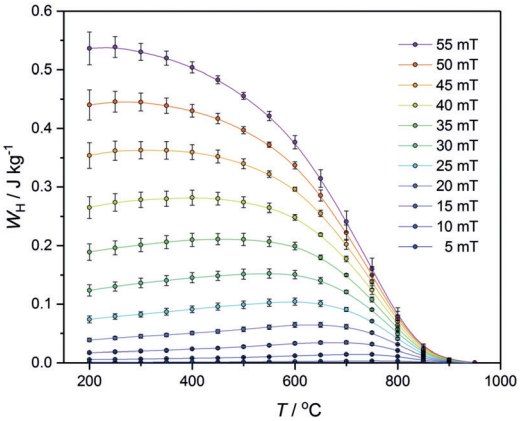

Figure 4. Field dependence of hysteresis heating per loop cycle for **CoNi** obtained from hysteresis measurements performed at temperatures between 200 °C and 950 °C at the indicated values of B_{max}. Error bars represent standard deviations calculated for four consecutive runs. Solid lines are guides to the eyes.

Identical measurements on **Cu⊂CoNi** reveal a similar hysteretic behavior, which is not surprising given the similar magnetization curves (Supporting Information, Figures S15,S16). A reactor setup dedicated for induction-heated SMR was designed and used for the testing of these catalysts under operating conditions (see the Supporting Information). A reactor made of quartz was implemented to avoid any

magnetic shielding effects. Based on the composition of the outlet gas, the SMR equilibrium temperature, energy transfer, and conversion of feed was calculated. For both **CoNi** and **Cu⊂CoNi**, the calculated energy transfer to the process gas was around 3–20 W g^{-1}, (averaged over a sample mass of 10 g) as estimated from the change in enthalpy, depending on the flow-rate of reactants however, the actual transfer to the reactor may be higher owing to heat losses associated with the reactor insulation. In all measurements, a frequency of 69 kHz and field amplitudes of up to 42 mT was used. For simplicity, only flow rates of 51 and 152 Nl h^{-1} are shown in Figure 5 (for a full view, see the Supporting Information, Figures S17 and S18).

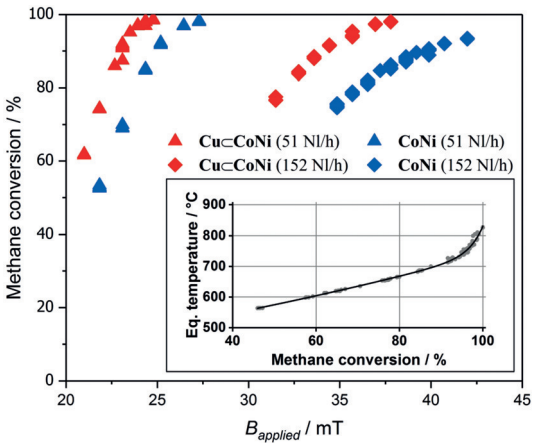

Figure 5. Influence of methane-flow on the conversion of CH_4 in the steam reforming reaction for a gas mixture treated over **CoNi** (blue) and **Cu⊂CoNi** (red) as a function of applied magnetic field. Inset: steam reforming equilibrium temperature as function of methane conversion at the experimental conditions. Inlet temperature ca. 200 °C, S/C ≈ 2, $P \approx 0$ bar gauge. Gas composition is as explained in the text and the Supporting Information.

Traditionally, the limiting factor on the reaction rate in industrial type externally heated reformer tubes is not the catalyst activity but the heat transfer to the catalyst.[19] This means that effectively only 10 %, or less, of the catalyst activity is utilized, the rest being lost owing to transport restrictions of the heat flux in the reactor bed.[27]

Interestingly, the data for **CoNi** and **Cu⊂CoNi** showed the CH_4 conversion increasing with magnetic field until a certain point where the increase in field is accompanied only by a small increase in H_2. For certain gas flows, this maximum is reached at full conversion (equilibrium). The curvature observed on approaching equilibrium is caused by the catalyst operating at the kinetic limit, that is, the catalyst is limited by reaction kinetics and not by the heat transfer (Figure 5). This is an important observation, as it is in stark contrast to the externally fired case. Additionally, owing to the improved activity of **Cu⊂CoNi**, 95 % conversion of methane to hydrogen was realized using roughly 15 % smaller applied magnetic fields as compared to **CoNi** for flows of 152 Nl h^{-1}.

The robustness of **CoNi** was evaluated in a prolonged experiment with a constant flow-rate of 101 Nl h^{-1} with a feed gas mixture of 29.7 % CH_4, 59.5 % H_2O, and 10.8 % H_2 (mol %), an input temperature of 237 °C, at close to atmospheric pressure, under an applied magnetic field of about 32 mT and a frequency of 69 kHz. Under these conditions, the conversion of methane was 90–95 %, corresponding to an equilibrium temperature of 715 °C. In the time frame of the experiment, which was more than 300 h, no significant decrease of the activity was observed as evidenced by the constant value of the methane conversion (Figure 6, red data

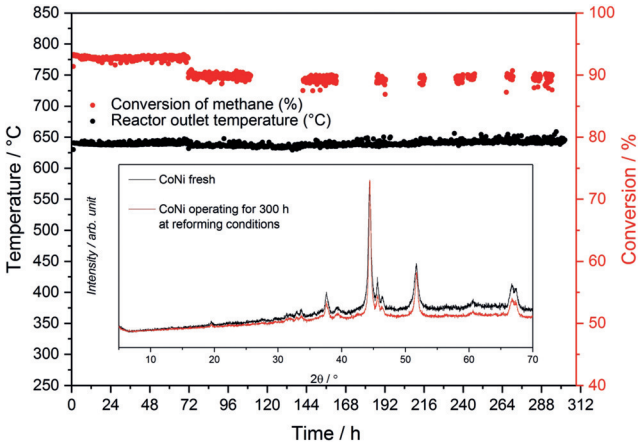

Figure 6. Overview of prolonged reforming experiment on **CoNi** using the induction-heated setup discussed in the text. No loss of activity is seen within the time frame of the experiment. The bump observed at $t = 72$ h is due to instrumental instabilities (see text). Inset: the XRD diffractogram before and after the experiment. For a larger view, see the Supporting Information, Figure S19.

points). The recorded time interval (ca. 14 days) is clearly much shorter than a typical reactor lifetime (years), but on the other hand, it is the time interval where most changes to the catalyst would be expected to occur. The drop observed in CH_4 conversion at 72 h is a result of water contamination of the gas chromatograph (GC) caused by a short power outage and does not represent an actual loss of catalyst performance. To avoid further damage, GC measurements after this point were performed in steps, roughly 24 h apart. The reactor outlet temperature was measured constantly throughout the experiment (black data points) using a Type-K thermocouple as described in the Supporting Information. Subsequently, the catalyst was unloaded and checked for changes in composition by XRD, ICP and STEM (Figure 2; Supporting Information, Figures S19–S21). All of these results underline the remarkable stability of the NP material, as no structural changes were found in addition to no carbon formation and no change of the Co wt % ratio, which was practically unchanged at 51.8 wt % (±2.0 wt %; Figure 2).

In summary, the preparation of a new chemically tailored nanostructured system was presented and its use in induction heated SMR was demonstrated. The chemical synthesis of metallic NPs allowed for the controlled production of a sample with a uniform and predictable Ni-Co alloy composition. Compared to previous ideas,[25] the realization of well-defined NPs through chemical synthesis led to an

increase in both hysteresis opening and steam reforming catalytic activity, presumably caused by a larger fraction of the NPs being ferromagnetic at the elevated reaction temperature. As a result, a marked increase was found in the efficiency of the NPs in terms of energy conversion under induction-heated steam reforming using only a magnetic field generated from electrical current as a power source.

With similar or even slightly inferior magnetic properties, **Cu⊂CoNi** demonstrated significantly improved reforming properties compared to **CoNi**, opening up for the possibility of producing even better catalysts by engineering the reactivity, as this is presently the limiting factor. Finally, we show the stability of chemically synthesized NPs to be excellent, and essentially inert to degradation in the first 300 h of operating at reforming conditions. Examining the CH_4 conversion under such conditions revealed that kinetic effects alone and not thermodynamics hampered the catalyst, opposed to the case of externally fired SMR, highlighting the excellent heat transfer from the induction field to the magnetic susceptor and active catalyst.

Combining chemically robust NPs with induction-heated catalysis may prove useful for many other industrial reactions, as the NPs can be modified to contain whatever active metal may be needed, and the operating temperature controlled by adjusting the applied field.

The implementation of induction heating in SMR may eliminate expensive waste-heat sections used in traditional methane reforming setups, significantly reducing the complexity of the process design and has the potential to drastically lower CO_2 emissions from the process.[28] This, together with the possibility of fast plant startup, holds promise for these materials as competitors for classical hydrogen plants or as part of ammonia plants in a future hydrogen economy and especially for ad hoc small-scale demands.

Acknowledgements

This work was partly funded by The University of Copenhagen, Haldor Topsøe A/S, the CoNeXT project and Innovation Fund Denmark (IFD) under File No. 5160-00004B. A PCT patent has been approved based on the results obtained.

Conflict of interest

The authors declare no conflict of interest.

Keywords: heterogeneous catalysis · hysteresis · induction heating · nanoparticles · steam reforming

How to cite: *Angew. Chem. Int. Ed.* **2018**, *57*, 10569–10573
Angew. Chem. **2018**, *130*, 10729–10733

[1] M. S. Yavuz, Y. Cheng, J. Chen, C. M. Cobley, Q. Zhang, M. Rycenga, J. Xie, C. Kim, K. H. Song, A. G. Schwartz, et al., *Nat. Mater.* **2009**, *8*, 935–939.
[2] B. P. Timko, K. Whitehead, W. Gao, D. S. Kohane, O. Farokhzad, D. Anderson, R. Langer, *Annu. Rev. Mater. Res.* **2011**, *41*, 3.1–3.20.
[3] H. Huang, S. Delikanli, H. Zeng, D. M. Ferkey, A. Pralle, *Nat. Nanotechnol.* **2010**, *5*, 602–606.
[4] N. W. Shi Kam, M. O'Connell, J. A. Wisdom, H. Dai, *Proc. Natl. Acad. Sci. USA* **2005**, *102*, 11600–11605.
[5] P. Cherukuri, E. S. Glazer, S. A. Curley, *Adv. Drug Delivery Rev.* **2010**, *62*, 339–345.
[6] M. N. Pérez-Camacho, J. Abu-Dahrieh, D. Rooney, K. Sun, *Catal. Today* **2015**, *242*, 129–138.
[7] "Ferromagnetic Materials for Induction Heated Catalysis": M. G. Vinum, P. M. Mortensen, PCT: WO 2017/186608 A1, **2017**.
[8] M. McCoy, M. Reisch, A. H. Tullo, P. L. Short, J.-F. Tremblay, W. J. Storck, *Chem. Eng. News* **2005**, *83*, 67–76.
[9] A. T-Raissi, D. L. Block, *IEEE Power Energy Mag.* **2004**, *2*, 40–45.
[10] J. R. Rostrup-Nielsen, J. Sehested, J. K. Nørskov, *Adv. Catal.* **2002**, *47*, 65–139.
[11] N. R. Udengaard, *Prepr. Pap. Am. Chem. Soc. Div. Fuel Chem.* **2004**, *49*, 906–907.
[12] J. R. Rostrup-Nielsen, L. J. Christiansen, *Concepts in Syngas Manufacture*, Imperial College Press, London, **2011**.
[13] S. Ceylan, C. Friese, C. Lammel, K. Mazac, A. Kirschning, *Angew. Chem. Int. Ed.* **2008**, *47*, 8950–8953; *Angew. Chem.* **2008**, *120*, 9083–9086.
[14] J. Wegner, S. Ceylan, C. Friese, A. Kirschning, *Eur. J. Org. Chem.* **2010**, 4372–4375.
[15] S. Ceylan, L. Coutable, J. Wegner, A. Kirschning, *Chem. Eur. J.* **2011**, *17*, 1884–1893.
[16] J. García-Aguilar, J. Fernández-García, E. V. Rebrov, M. R. Lees, P. Gao, D. Cazorla-Amorós, Á. Berenguer-Murcia, *Chem. Commun.* **2017**, *53*, 4262–4265.
[17] Y. Liu, N. Cherkasov, P. Gao, J. Fernández, M. R. Lees, E. V. Rebrov, *J. Catal.* **2017**, *355*, 120–130.
[18] A. Meffre, B. Mehdaoui, V. Connord, J. Carrey, P. F. Fazzini, S. Lachaize, M. Respaud, B. Chaudret, *Nano Lett.* **2015**, *15*, 3241–3248.
[19] A. Bordet, L. M. Lacroix, P. F. Fazzini, J. Carrey, K. Soulantica, B. Chaudret, *Angew. Chem. Int. Ed.* **2016**, *55*, 15894–15898; *Angew. Chem.* **2016**, *128*, 16126–16130.
[20] J. M. Leger, C. Loriers-Susse, B. Vodar, *Phys. Rev. B* **1972**, *6*, 4250–4261.
[21] I. Barin, *Thermochemical Data of Pure Substances*, VCH, Weinheim, **1989**.
[22] J. R. Rostrup-Nielsen in *Catalysis—Science and Technology* (Eds.: J. R. Anderson, M. Boudart), Springer, Berlin, **1984**.
[23] C. Perego, P. Villa, *Catal. Today* **1997**, *34*, 281–305.
[24] J. A. Schwarz, C. Contescu, A. Contescu, *Chem. Rev.* **1995**, *95*, 477–510.
[25] P. M. Mortensen, J. S. Engbæk, S. B. Vendelbo, M. F. Hansen, M. Østberg, *Ind. Eng. Chem. Res.* **2017**, *56*, 14006–14013.
[26] J. Barcicki, A. Denis, W. Grzegorczyk, D. Nazimek, T. Borowiecki, *React. Kinet. Catal. Lett.* **1976**, *5*, 471–478.
[27] K. Aasberg-Petersen, J. H. Bak Hansen, T. S. Christensen, I. Dybkjaer, P. S. Christensen, C. S. Nielsen, S. E. L. W. Madsen, J. R. Rostrup-Nielsen, *Appl. Catal. A* **2001**, *221*, 379–387.
[28] N. Muradov, F. Smith, C. Huang, A. T-Raissi, *Catal. Today* **2006**, *116*, 281–288.

Manuscript received: April 26, 2018
Revised manuscript received: May 25, 2018
Accepted manuscript online: June 19, 2018
Version of record online: July 13, 2018

